Morphological Distribution and Phase Composition of Rare Earth Elements in Waste Incineration Fly Ash

Hong Cui[1]*, Qiaoyan Qin[2]*

[1] College of Geographical Science, Shanxi Normal University, 041000 Linfen, China
[2] Center of Analysis and Test, Shanxi Normal University, 041000 Linfen, China

* Correspondence: Hong Cui (cuihong@sxnu.edu.cn); Qiaoyan Qin (18100349595@163.com)

Abstract: Utilising scanning electron microscopy (SEM) and X-ray powder diffraction (XRD), the morphological and phase composition characteristics of waste incineration fly ash were meticulously analysed. Morphological evaluations revealed a predominant presence of irregularly shaped particles, encountering a spectrum of structures inclusive of polycrystalline polymers and amorphous forms. Additional particle shapes encompassed polygons, strips, blocks, and flakes, while a notable high porosity between particles and a markedly rough surface were observed. Despite the scarcity of complete crystals within the ash, the majority manifested as polycrystalline polymers and amorphous forms, indicating the structural complexity intrinsic to waste incineration fly ash. Through the deployment of chemical continuous extraction technology, forms, migrations, and transformation laws pertaining to rare earth elements (REEs) in fly ash were elucidated. In three fly ash samples analysed for REEs, the most abundant state was identified as the residual, succeeded by the Fe-Mn oxide-bound state and minimally, the carbonate-bound state. Amongst all REEs, Ce exhibited the highest prevalence, followed by La, Y, Nd, Gd, and other elements. Furthermore, the source of waste and the respective incineration process markedly influenced REEs content.

Keywords: Municipal solid waste; Rare earth elements; Incineration fly ash; Morphological distribution

1 Introduction

In recent years, the development of municipal solid waste (MSW) incineration as a disposal method has been marked by notable expansion, owing largely to its efficacy in mass and volume reduction of MSWs and its capacity for heat production, utilised in electricity or steam generation worldwide [1, 2]. In China, a substantial increment in the employment of MSW incineration treatment is observed annually. However, the residues from solid waste incineration, notably, fly ash, bottom ash, and cinder—which collectively constitute approximately 30%-35% of refuse weight—are predominantly subjected to elementary treatment methods, such as isolated landfilling. Such methodologies harbour potential hazards [3–7].

Fly ash, comprising about 5% of waste, is designated as hazardous, attributed to its fine particle composition and proficiency in absorbing substantial quantities of toxic and detrimental substances, including heavy metals and dioxins [3]. Statistical data highlight that approximately 600,000 tons of fly ash are emitted annually from waste incineration plants in the Beijing-Tianjin-Hebei region alone. Moreover, projections denote that, by 2020, China will witness an annual fly ash emission surpassing 10 million tons [5–7].

REEs, often regarded as the "vitamins of modern industry" and the "treasure house of new materials," have emerged as indispensable strategic materials, pivotal for the evolution of new and high technologies, advanced national defence technologies, and the metamorphosis of traditional industries globally [8, 9]. Owing to the REEs' intricate composition, structural complexity, and chemically analogous properties, coupled with the minuscule separation coefficient of adjacent elements, their separation and purification into singular elements have been rendered exceedingly challenging, necessitating significant energy and resource expenditure [10–12].

The extraction of REEs from mining not only precipitates serious ecological and environmental conundrums but also propels the continual scarcity of rare earth resources [13, 14]. Consequently, the recycling of REEs has emerged as a pivotal avenue for establishing a sustainable development strategy, with potential to confer immense social, economic, and environmental benefits [15, 16]. Recent research endeavors have centred on the extraction of REEs

https://doi.org/10.56578/atg020304

from various waste sources, such as production wastewater, waste residue, waste material, and end-of-life electronic products. Notably, an uptick in studies focusing on REEs extraction from coal ash has been observed [17–23].

In the United States and Russia, pragmatic technologies for extracting REEs from coal ash have been developed and implemented [24, 25]. Given that MSWs encapsulate an assortment of everyday items imbued with REEs, the high-temperature incineration of MSWs frequently results in a significant concentration of REEs in the residues. These REEs predominantly exist in the form of rare earth oxides (REO) and chlorides, thereby simplifying subsequent REEs separation and purification procedures and technologies, and mitigating extraction difficulties [26].

A standardised procedure for studying REEs in waste incineration residues remains elusive, despite both coal ash and these residues emerging from high-temperature combustion processes. Noteworthy differences exist between the enrichment characteristics and morphological distributions of REEs in coal and waste. The primary influence on REEs in coal is geological formation, while in waste, REEs, having been artificially added and significantly purified, present different challenges and opportunities [15].

Sparse reports do illuminate some aspects of REEs in fly and bottom ash from both medical waste and MSW incineration. Investigations into REEs characteristics and environmental impacts from diverse MSW incinerators across four Chinese cities revealed substantial variations in total REE content in fly ash, ranging from 10.2 to 78.9 mg/kg, and demonstrated distinct distribution patterns for various REEs [27]. A study [28] spotlighted the feasibility of achieving industrial extraction levels of REEs enrichment in fly ash.

It is acknowledged that REEs manifest differently across varied geological bodies and environmental conditions. Their distribution characteristics in rocks, minerals, and waste materials serve as a crucial foundation for developing REEs separation and purification technologies [29]. Moreover, understanding the enrichment law and morphological distribution characteristics of REEs in waste incineration fly ash not only guides the selection of extraction technology and methods but also furnishes valuable data for studying the migration and transformation behaviour of REEs [30–32]. While fly ash is characterised through elemental analysis, XRD, SEM-EDS, and BET surface area and their implications discussed for subsequent REEs extraction processes, the distribution characteristics of REEs in fly ash and bottom ash from waste incineration are scarcely reported [14].

Therefore, discerning the distribution of REEs in fly ash is imperative to formulate efficacious REEs extraction methodologies from this burgeoning resource. The occurrence state of REEs in waste incineration fly ash has been identified, utilising the chemical continuous extraction method of heavy metal elements prevalent in environmental chemistry, and harmonised with the microstructure and phase composition characteristics of fly ash. This approach provides a foundational basis for examining trace distribution, evaluating recovery rates, and developing resource recovery technologies for REEs throughout the waste incineration process.

2 Materials and Methods

2.1 Sampling

Three varieties of fly ash samples were collected: bag filter fly ash (S1) and flue fly ash (S2) from a domestic waste incineration plant in Beijing, and mixed fly ash (S3) from a similar plant in Shanxi Province. During stable operations of the incinerators, fly ash samples were procured and stored in clean plastic bags. Subsequently, the samples were transported to the laboratory and refrigerated at a low temperature until further use.

2.2 Experimental Apparatus and Methods

2.2.1 Micromorphology analysis

The microstructure of fly ash was analysed utilising a jSM-7500F SEM from Rigaku, Japan, and an OXFORD INCA PentaFET×3 energy spectrometer from the UK. SEM working conditions included an accelerating voltage of 20 KV, a probe current of 10, and WD8 mm. For the energy spectrometer, point analysis acquisition time was set at 180 s. To enhance the electrical conductivity of the sample, the sample surface was gold-sprayed. Backscattered electron images facilitated sample observation, from which high-brightness particles were selected. The REEs were subsequently detected via the magnifying energy spectrometer, enabling the capture of second-order electron images and backscattered electron images. These images and their associated energy spectra were harnessed to analyse the morphologies and structural characteristics of the fly ash.

2.2.2 Phase composition characteristics

Phase composition characteristics of the fly ash samples were discerned using an Ultima IV-185 X-ray diffractometer from Rigaku, Japan. Operational parameters of the X-ray powder diffractometer included a Cu target, test voltage of 40 keV, test current of 40 mA, and utilisation of a scintillation counter in continuous scanning mode. The sweep range was set between 4° and 100°, with a scanning speed of 2°/min. The resultant charts from experimental tests were processed using Jade 6.0 software.

2.2.3 Morphological characteristics

REEs in fly ash samples were extracted into five sequential fractions using the Tessier separation and extraction method, specifically: (I) the exchangeable state, (II) bound to carbonate, (III) bound to Fe–Mn oxides, (IV) bound to organic matters, and (V) the residual fraction. The explicit operational process was modelled on the modified Tessier scheme [33–35]. REEs content was quantitatively analysed via microwave digestion/inductively coupled plasma mass spectrometry (ICP-MS) [36, 37], employing a NexION 300X ICP-MS instrument from PerkinElmer. All glassware used in the experiments was subjected to soaking in a 5% nitric acid solution for a minimum of 24 hours, followed by extensive washing with deionised water, and subsequent drying in an oven for later usage.

3 Results and Discussion

3.1 SEM Analysis

In the encompassed SEM images, represented in Figures 1-3, the electron microscopy visuals of three distinct fly ash samples are depicted at magnifications of 200x (left image) and 3000x (right image). Notably, each set of images provides insightful data regarding the microstructural properties of different fly ash samples (S1, S2, and S3).

In the S1 sample, particles of fly ash were observed to be uniformly distributed, exhibiting simplicity in type and finesse in form. Predominantly, spherical flocculent aggregates, characterised by diminutive pores and a smooth surface, were discerned. Contrarily, the S2 fly ash samples predominantly exhibited amorphous flocculent particles, denoting a dense interior, adorned with small particles on the surface, numerous pores, and a coarse surface texture. A notable distinction was identified in particle size between S1 and S2, with the latter presenting significantly smaller particles. The S3 fly ash samples displayed a morphological diversity inclusive of varied shapes—round, polygonal, strip, block, and flake—with heightened porosity observed between particles and a rugged surface exterior.

In a comprehensive perspective, few complete crystals were identified in the fly ash, with the majority presenting in polycrystalline polymer and amorphous forms, highlighting the complex structural nature of fly ash derived from waste incineration. Evidently, disparate incineration technologies, incinerator types, and waste sources wield substantial influence on the properties of fly ash [5].
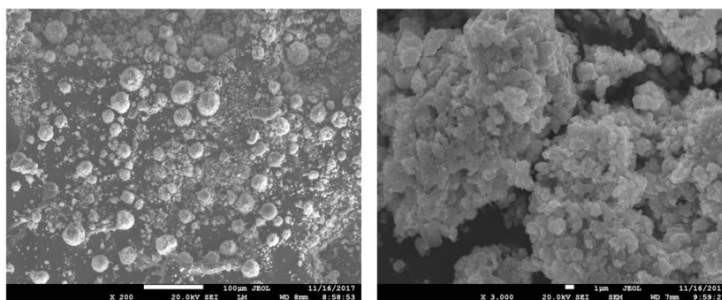

Figure 1. Scanning electron micrograph of the S1 sample
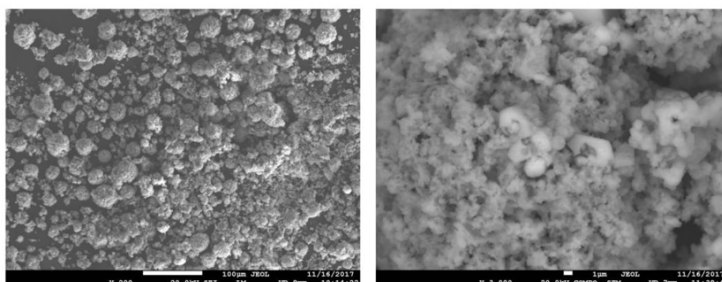
Figure 2. Scanning electron micrograph of the S2 sample

3.2 XRD Analysis

Figure 4 elucidates the XRD patterns of samples S1, S2, and S3, revealing several critical insights into the main mineral components embedded within the fly ash, which were identified to include SiO_2, $CaCO_3$, $CaSO_4$, $Ca_2Al_2SiO_7$, Fe_2O_3, Fe_3O_4, Al_2O_3, and Al_2SiO_4. Besides these primary mineral compositions, additional substances such as
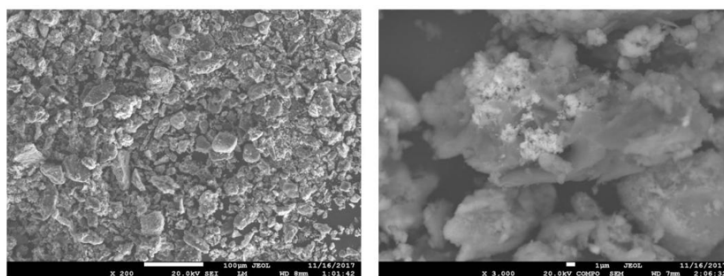
Figure 3. Scanning electron micrograph of the S3 sample

$NaCl$, KCl, $MgSiO_3$, CaO, Mg_2SiO_4, $NaAlSiO_4$, $MgAl_2Si_3O_{10}$, $Ca(OH)_2$, $BaSO_4$, FeO, FeS_2, $NaSO_4$, and others were detected, encompassing over 20 different phase types. Noteworthy is the significant detection of SiO_2 across all three fly ash samples.

In all three samples, a notably high content of the glass phase, exceeding 58%, was observed. This high percentage is attributed to the transformation of certain substances within the garbage into a molten state during the high-temperature incineration process. These liquid-phase molten substances, upon cooling and without sufficient time to crystallize, were transferred to the fly ash, culminating in a relatively elevated glass state. This is corroborated by Lin et al. [38], who highlighted this as a principal reason for the elevated activity observed in fly ash.
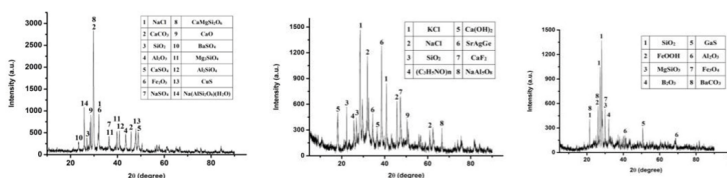

Figure 4. XRD pattern

A conspicuously elevated content of SiO_2 in sample S3, in comparison to S1 and S2, was discerned. This can be ascribed to the fact that S3 emanates from a waste incineration plant employing a fluidized bed waste incinerator process, necessitating the addition of coal for fuel combustion and, consequently, resulting in an augmented content of fly ash [39]. Contrastingly, samples S1 and S2 exhibited relatively high Cl content compared to S3, a phenomenon potentially related to the nature of the waste source, perhaps attributable to the elevated content of chlorine-containing organic products in the garbage derived from more developed areas.

The presence of metallic elements, namely Fe, Cu, Pb, Zn, Cr, and Cd, was identified across all three fly ash samples, ordered in decreasing content as follows: Fe > Cu > Pb > Zn > Cr > Cd. During the high-temperature incineration process, these elements are capable of forming low-boiling-point, high-volatility metal chlorides through combination with chlorine atoms, concentrating on the fly ash surface during the flue gas condensation process. Consequently, these heavy metals are found in considerable quantities in the fly ash. Moreover, it is proposed that lithophile elements such as Cu and Cr may be transported into the fly ash via solid particles.

3.3 Qualitative Analysis of Rare Earth Particles

Utilisation of SEM/energy-dispersive X-ray spectroscopy (SEM/EDS) facilitated simultaneous observation and qualitative analysis of the morphology and elemental composition of the examined samples. Analyses of the three distinct fly ash samples are depicted in Figure 5, Figure 6, and Figure 7, wherein each set sequentially presents secondary electron images, backscattered electron images, and energy spectrum images of rare earth particles.
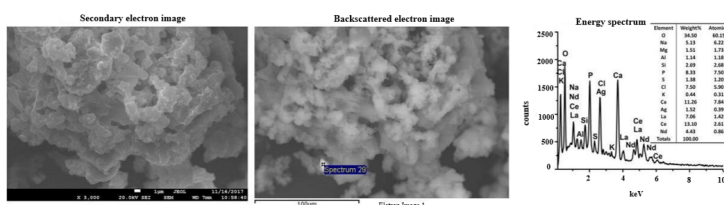

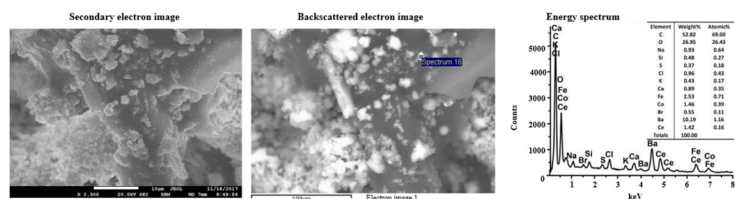**Figure 5.** SEM/EDS analysis of rare earth particles in sample S1

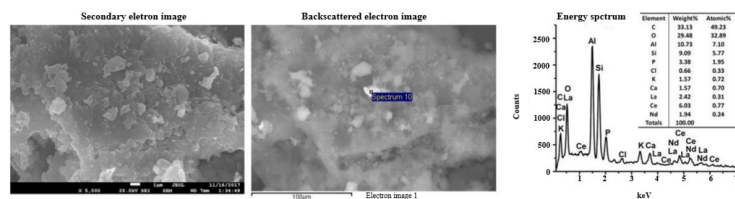**Figure 6.** SEM/EDS analysis of rare earth particles in sample S2

Figure 7. SEM/EDS analysis of rare earth particles in sample S3

In all fly ash samples, the presence of REEs was confirmed. Specifically, particles encompassing Ce, La, Nd, and further Ce were identified in samples S1 and S2, while particles containing Ce, La, and Nd were discerned in S3. Predominantly, these rare earth particles exhibited spherical or circular morphologies, with particle sizes consistently ranging between 1 and 2 μm.

Furthermore, critical insights into the elemental composition were derived from the energy spectra of the samples. For instance, S1 revealed prominent peaks for O, Ca, P, Na, Si, and Cl, indicating their significant presence within. Conversely, S2 demonstrated elevated contents of C, O, Ba, Fe, Co, and Cl, while S3 was characterised by high contents of C, O, Al, Si, P, and Ca. It was noted that the Cl content in samples S1 and S2 surpassed that in S3, maintaining consistency with prior observations.

The notable content of Ba in S2 may be attributable to the incorporation of alloys and scrap bearings from the metallurgical industry into the construction waste. The relatively large proportion of Ba, which is predisposed to being deposited in flue ash, underscores this hypothesis [21]. Moreover, the elevated Al content in S3 may be a consequence of the proximity of aluminium processing plants to the waste incineration plant, implicating the incineration waste in containing a substantial Al residue.

3.4 Morphological Distribution Characteristics

3.4.1 Morphology distribution of REEs in S1

Table 1 delineates both the aggregate and morphological-specific content of 15 REEs in sample S1. A substantial variance in the morphological distribution of REEs in S1 was observed. Predominantly, the residual state was identified as the principal form, boasting a content of 162.7769 mg/kg, which constitutes a significant 91.48% proportion. Subsequently, the iron and Fe–Mn oxides-bound state emerged as prevalent, documented at 13.2423 mg/kg and accounting for 7.44% of the total. These two morphologies collectively represented over 98% of the total REE content. Alternatively, the exchangeable state and the organic matter-bound state were identified as minor constituents, contributing 0.62% and 0.42% respectively. Negligible was the bound to carbonate state, documented at a mere 0.0687 mg/kg and representing less than 0.01% of the total.

An evaluation of the collective distribution of the 15 REE species revealed notable concentrations of Ce, La, Y, Nd, Yb, Gd, and Pr in S1, each accounting for more than 1% and aggregating to 96.96% of the overall total. Ce emerged dominant, with a concentration of 136.1708 mg/kg, and encompassing 76.52% of the total. La, Y, and Nd were evidenced to contribute 5.75%, 5.48%, and 4.73%, respectively.

Upon examining the residual REEs of S1, an exceedingly dominant presence of Ce was ascertained, constituting a substantial 79.94%, while all other elements manifested proportions below 10%. Y, La, and Nd comprised 5.15%, 4.15%, and 3.96%, respectively. In the Fe-Mn oxide state, Ce demonstrated the highest concentration at 5.0820 mg/kg, accounting for 38.38%. La followed at 23.89% and Nd at 14.01%. All other REEs registered under 10%, with Y and Pr documenting 8.97% and 3.99%, respectively. Within the exchangeable state, Ce maintained dominance at 61.11%, followed by La (13.34%), Nd (9.47%), Y (5.73%), and Pr (2.85%), while all remaining REEs recorded under 2%. In the organic binding state, Ce, La, Y, and Nd exhibited more than 10%, with Ce documenting the highest proportion at 41.83%. All other REEs revealed minimal contributions, constituting less than 5%.

Table 1. Diverse forms of REEs in S1 samples (mg/kg)

Element	I	II	III	IV	V	Total Content
Ce	0.4573	0.0268	5.0820	0.4602	130.1444	136.1708
Pr	0.0213	0.0007	0.5287	0.0303	1.6630	2.2438
Tb	0.0017	0.0000	0.0509	0.0054	0.2674	0.3254
Ho	0.0018	0.0003	0.0396	0.0044	0.2493	0.2955
Er	0.0055	0.0003	0.1262	0.0153	0.8506	0.9978
Tm	0.0009	0.0000	0.0161	0.0020	0.1169	0.1359
Lu	0.0010	0.0001	0.0179	0.0026	0.1312	0.1528
Y	0.0429	0.0109	1.1874	0.1270	8.3757	9.7439
La	0.0998	0.0069	3.1638	0.1921	6.7604	10.2230
Sm	0.0129	0.0008	0.2936	0.0241	1.1726	1.5040
Eu	0.0116	0.0035	0.0883	0.0124	0.3986	0.5143
Dy	0.0084	0.0003	0.2148	0.0234	1.2378	1.4847
Yb	0.0065	0.0002	0.1973	0.0232	2.8570	3.0841
Gd	0.0058	0.0153	0.3807	0.0547	2.1921	2.6486
Nd	0.0709	0.0026	1.8550	0.1231	6.3599	8.4115
Total	0.7483	0.0687	13.2423	1.1002	162.7769	177.9361

3.4.2 Morphology distribution of REEs in S2

Table 2 articulates the cumulative amount and morphological dissemination of 15 REEs in S2. Overall, the total REEs in S2 is approximately one-third of that observed in S1, potentially attributable to a propensity for REEs to concentrate in particles of a larger size. A marked difference in the morphological distribution of the various REEs was discerned in S2, with the residual state content emerging as paramount, constituting 61.43%. Subsequent in prevalence was the Fe-Mn oxide complex, accounting for 33.37%. Other forms were evidenced to be less abundant, with the organic combination state and exchangeable state representing 3.45% and 1.06% respectively. The carbonate binding state, although least prevalent at merely 0.7%, was deemed negligible. These characteristics demonstrate a semblance to those identified in S1.

An examination of the total distribution of 15 REEs indicated pronounced contents of Ce, La, Y, Nd, Gd, Pr, and Yb in S2. Specifically, Ce was evidenced at 29.4157 mg/kg, representing a substantial 76.52%. Meanwhile, La, Y, Nd, Gd, and Pr contributed 14.74%, 11.09%, 9.29%, 2.71%, and 2.55%, respectively.

In the residual REEs within S2, Ce was identified as the most predominant, comprising 62.75%, followed by La, Y, and Nd at 12.47%, 10.08%, and 6.05%, respectively. All remaining elements were evidenced at under 3%, with Gd and Pr contributing 2.14% and 1.76%, respectively. In the Fe-Mn oxide bound state, Ce maintained its dominance, accounting for 35.11%, with La, Nd, Y, Pr, and Gd contributing 18.63%, 14.97%, 12.82%, 3.97%, and 3.63%, respectively. Similar distribution patterns were observed amongst the REEs across the remaining morphologies.

Table 2. Contents of different forms of REEs in S2 sample (mg/kg)

Element	I	II	III	IV	V	Total Content
Ce	0.4369	0.2952	6.5548	0.5613	21.5674	29.4157
Pr	0.0117	0.0044	0.7409	0.0660	0.6042	1.4272
Tb	0.0004	0.0005	0.1122	0.0129	0.1040	0.2300
Ho	0.0004	0.0004	0.0930	0.0119	0.0656	0.1713
Er	0.0008	0.0008	0.2803	0.0392	0.2463	0.5673
Tm	0.0001	0.0003	0.0383	0.0052	0.0278	0.0717
Lu	0.0004	0.0002	0.0392	0.0062	0.0277	0.0737
Y	0.0159	0.0140	2.3940	0.3192	3.4632	6.2063
La	0.0750	0.0402	3.4785	0.3663	4.2870	8.2469
Sm	0.0052	0.0029	0.5467	0.0549	0.3965	1.0062
Eu	0.0037	0.0060	0.1709	0.0214	0.1612	0.3633
Dy	0.0018	0.0012	0.4702	0.0554	0.3702	0.8988
Yb	0.0014	0.0013	0.2772	0.0382	0.2363	0.5544
Gd	0.0015	0.0084	0.6773	0.0961	0.7340	1.5172
Nd	0.0356	0.0142	2.7943	0.2748	2.0779	5.1968
Total	0.5908	0.339	18.6678	1.929	34.3693	55.9468

3.4.3 Morphology distribution of REEs in S3

Table 3 delineates the morphological distribution and overall quantity of 15 REEs within S3. A discernible elevation in the REE content in S3 compared to S1 and S2 is evident. The augmentation of REE content is potentially twofold: initially, the fluidized bed waste incineration process necessitates the inclusion of coal for combustion; secondly, the refuse in this area encompasses a significant quantity of civil coal ash and solid waste from the coal chemical industry, signifying a substantial presence of REEs within the coal ash [26].

Distinct variations in the morphological distribution of REEs within S3 were observed. The residual REEs content was notably high, calculated at 1523.4791 mg/kg, and constituted 95.06%, markedly exceeding the other four forms. Subsequently, the Fe-Mn oxide binding state accounted for approximately 4.05%, summing these two states to represent over 99% of REEs. The remaining forms demonstrated lower content, where the organic binding state exhibited around 0.84%, the exchangeable state around 0.22%, and the carbonate binding state the least, merely 0.2%. Noteworthy is that the distribution of REEs in various forms shares similarities with those in S1 and S2.

According to the overarching distribution of the 15 REEs, elevated contents of Ce, La, Y, Nd, Gd, Pr, and Yb in S3 were identified. Specifically, Ce was presented at 1286.8986 mg/kg, contributing a striking 76.52%, while La, Y, Nd, and Gd constituted 7.70%, 5.17%, 2.80%, and 1.14% respectively, with the remaining elements registering minimal contents. In the residual REEs of S3, Ce emerged as the predominant element at 1253.3166 mg/kg, accounting for 82.27% of the total residual content, followed by La, Y, Nd, Gd, and Pr at 7.39%, 4.79%, 2.29%, 1.02%, and 0.53% respectively. The distribution of REEs in the four alternative morphologies was analogous.

Table 3. Contents of REEs in various forms in S3 sample (mg/kg)

Element	I	II	III	IV	V	Total Content
Ce	0.2416	0.2348	30.5854	2.5201	1253.3166	1286.8986
Pr	0.0068	0.0043	1.9671	0.5814	8.0193	10.5791
Tb	0.0005	0.0005	0.3096	0.1085	1.1347	1.5537
Ho	0.0007	0.0010	0.3591	0.1267	1.2190	1.7066
Er	0.0023	0.0014	1.0449	0.3919	4.4415	5.8820
Tm	0.0002	0.0002	0.1493	0.0557	0.6218	0.8272
Lu	0.0003	0.0003	0.1522	0.0591	0.7895	1.0013
Y	0.0211	0.0165	7.2890	2.5477	72.9986	82.8729
La	0.0284	0.0684	8.4658	2.2802	112.6314	123.4742
Sm	0.0044	0.0031	1.6781	0.5434	6.2136	8.4426
Eu	0.0028	0.0036	0.3804	0.1275	1.0814	1.5958
Dy	0.0022	0.0015	1.8018	0.6275	6.0451	8.4782
Yb	0.0014	0.0013	0.9798	0.3767	4.5813	5.9404
Gd	0.0050	0.0064	2.0775	0.7425	15.5487	18.3801
Nd	0.0222	0.0162	7.6527	2.4413	34.8364	44.9689
Total	0.3399	0.3596	64.8927	13.5302	1523.4791	1602.6016

Table 4 illustrates the distribution of light REEs (LREEs: La, Ce, Pr, Nd, Sm, Eu) and heavy REEs (HREEs: Tb, Ho, Er, Tm, Lu, Y, Dy, Yb, Gd) in three fly ash samples. LREEs were observed to be predominant, accounting for upwards of 80% of total REEs (Σ REEs) in the fly ash. This may be attributed to the enhanced volatility of LREEs, facilitating their enrichment in fly ash [25].

Table 4. Content of LREEs and HREEs in fly ash

Sort of REE	S1	S2	S3
LREE (mg/kg)	159.0675	45.6561	1475.9591
HREE (mg/kg)	18.8687	10.2908	126.6424
ΣREE(mg/kg)	177.9362	55.9468	1602.6016

In summary, the primary form of metal in fly ash derived from MSW incineration is residual. A prevailing consensus among scholars postulates that the stable existence of heavy metals within the crystal lattice of quartz and clay minerals can be categorized as residual heavy metals. These residual heavy metals, characterized by minimal activity, exhibit remarkable stability and present difficulty in release under typical conditions. Furthermore, Ce content in fly ash is pronouncedly elevated, significantly surpassing that of the other 14 REEs and even exceeding the crustal abundance of Ce (46.1 mg/kg) [26]. This may be attributed to the extensive utilization of the Ce element to optimize material performance across a range of applications, including glass, fuel cells, coloured plastics, paper, and non-ferrous metals.

4 Conclusions

The diversity in particle morphology across fly ash samples S1, S2, and S3 is elucidated through the present investigation. S1 exhibits a predominance of evenly distributed, finely granulated, and predominantly spherical flocculent aggregates, characterized by minimal porosity and a comparatively smooth surface. In contrast, S2 is predominantly comprised of amorphous flocculent particles, exhibiting a dense internal structure, multiple pores, adherence of smaller particles to their surface, and a notably rough surface texture. S3 demonstrates morphological richness, presenting not only spherical particles but also adopting polygonal, strip, block, and flake shapes, along with a high inter-particle porosity and a rough surface. Remarkably, the fly ash predominantly manifests in the form of polycrystalline polymers and amorphous forms, reflecting a complex structure resultant from waste incineration.

Comprehensive examination reveals the main mineral constituents of the fly ash to encompass SiO_2, $CaCO_3$, $CaSO_4$, $Ca_2Al_2SiO_7$, Fe_2O_3, Fe_3O_4, Al_2O_3, and Al_2SiO_4. A plethora of additional minerals is identified, including NaCl, KCl, $MgSiO_3$, CaO, Mg_2SiO_4, $NaAlSiO_4$, $MgAl_2Si_{13}O_{10}$, $Ca(OH)_2$, $BaSO_4$, FeO, FeS_2, and $NaSO_4$, with the content of the glass phase reaching up to 58% across all three fly ash samples..

A synergy of qualitative analysis and SEM/EDS establishes that S1 harbours elements such as Ce, La, and Nd, while S2 is recognized to contain Ce elements. S3 is discerned to encompass Ce, La, Nd, and additional particles of distinct elements. Predominantly spherical or circular, most rare earth particles are discerned to fall within a size range of 1-2μm. Notably, Ce, La, and Nd emerge as substantial contributors to the REEs composition in the fly ash, corroborating findings derived from ICP-MS determination.

ICP-MS analysis unveils a notable variance in the total REEs across fly ash derived from disparate incineration processes, waste sources, and distinct parts. A disparity is also evident in the distribution of distinct REEs. Collectively, Ce emerges as the most predominant element, followed sequentially by La, Y, Nd, and Gd. The REEs content in S3 is observed to considerably surpass that in S1 and S2, a phenomenon primarily attributed to the substantial presence of REEs in coal ash.

Morphological analysis of REEs articulates the highest content is in the residual state across the three fly ash samples, followed by the Fe-Mn oxide bound state, and culminating with the carbonate bound state witnessing the lowest representation. A congruent distribution of different REEs across the five forms is perceptible.

Data Availability

The authors declare that they have no known competing financial interests or personal relationships that could have appeared to influence the work reported in this paper.

Acknowledgment

Conflicts of Interest

The authors declare that they have no conflicts of interest.

References

[1] M. L. Xu, J. H. Yan, Z. Y. Ma, Q. Wang, W. Sun, and K. F. Cen, "Characteristics investigation of the solid residues from cfb municipal solid waste incinerator," *Zhongguo Dianji Gongcheng Xuebao(Proceedings of the Chinese Society of Electrical Engineering)*, vol. 27, no. 8, pp. 16–21, 2007.

[2] R. D. Zheng, L. Y. Yuan, S. Q. Tang, and F. Wang, "Characteristic analysis of fly ash from municipal solid waste incineration in Hangzhou," *Environ. Sanit. Eng.*, vol. 24, no. 4, pp. 44–45, 2016.

[3] V. Funari, R. Braga, S. N. Bokhari, E. Dinelli, and T. Meisel, "Solid residues from italian municipal solid waste incinerators: A source for "critical" raw materials," *Waste Manag.*, vol. 45, pp. 206–216, 2015. https://doi.org/10.1016/j.wasman.2014.11.005

[4] W. Li, K. Gu, Q. Yu, Y. Sun, Y. Wang, M. Xin, R. Bian, H. Wang, Y. N. Wang, and D. Zhang, "Leaching behavior and environmental risk assessment of toxic metals in municipal solid waste incineration fly ash exposed to mature landfill leachate environment," *Waste Manag.*, vol. 120, pp. 68–75, 2020. https://doi.org/10.1016/j.wasman.2020.11.020

[5] Y. Pan, Z. Wu, J. Zhou, J. Zhao, X. Ruan, J. Liu, and G. Qian, "Chemical characteristics and risk assessment of typical municipal solid waste incineration (MSWI) fly ash in china," *J. Hazard. Mater.*, vol. 261, pp. 269–276, 2013. https://doi.org/10.1016/j.jhazmat.2013.07.038

[6] S. Wu, J. Zhou, Y. Pan, J. Zhang, L. Zhang, N. Ohtsuka, M. Motegi, S. Yonemochi, K. Oh, S. Hosono, and G. Qian, "Dioxin distribution characteristics and health risk assessment in different size particles of fly ash from MSWIs in China," *Waste Manag*, vol. 50, pp. 113–120, 2016. https://doi.org/10.1016/j.wasman.2016.01.038

[7] X. F. Sun, J. H. Li, X. D. Zhao, B. L. Zhu, and G. L. Zhang, "A review on the management of municipal solid waste fly ash in American," *Procedia Environ. Sci.*, vol. 31, pp. 535–540, 2016. https://doi.org/10.1016/j.proenv.2016.02.079

[8] T. Dutta, K. H. Kim, M. Uchimiya, E. E. Kwon, B. H. Jeon, A. Deep, and S. T. Yun, "Global demand for rare earth resources and strategies for green mining," *Environ. Res.*, vol. 150, pp. 182–190, 2016. https://doi.org/10.1016/j.envres.2016.05.052

[9] B. Sprecher, I. Daigo, S. Murakami, R. Kleijn, M. Vos, and G. J. Kramer, "Framework for resilience in material supply chains, with a case study from the 2010 rare earth crisis," *Environ. Sci. Technol*, vol. 49, pp. 6740–6750, 2015. https://doi.org/10.1021/acs.est.5b00206

[10] R. K. Jyothi, T. Thenepalli, J. W. Ahn, P. K. Parhi, K. W. Chung, and J. Y. Lee, "Review of rare earth elements recovery from secondary resources for clean energy technologies: Grand opportunities to create wealth from waste," *J. Clean. Prod.*, vol. 267, p. 122048, 2020. https://doi.org/10.1016/j.jclepro.2020.122048

[11] R. Lin, M. Stuckman, B. H. Howard, T. L. Bank, E. A. Roth, M. K. Macala, C. Lopano, Y. Soong, and E. J. Granite, "Application of sequential extraction and hydrothermal treatment for characterization and enrichment of rare earth elements from coal fly ash," *Fuel*, vol. 232, pp. 124–133, 2018. https://doi.org/10.1016/j.fuel.2018.05.141

[12] J. Pan, C. Zhou, C. Liu, M. Tang, S. Cao, T. Hu, W. Ji, Y. Luo, M. Wen, and N. Zhang, "Modes of occurrence of rare earth elements in coal fly ash: A case study," *Ener. Fuels*, vol. 32, pp. 9738–9743, 2018. https://doi.org/10.1021/acs.energyfuels.8b02052

[13] H. He, C. Fan, Q. Peng, M. Wu, J. Zheng, and G. L. Wu, "Bioaccumulation and translocation of rare earth elements in two forage legumes grown in soils treated with coal fly ash," *Chem. Geol.*, vol. 528, p. 119284, 2019. https://doi.org/10.1016/j.chemgeo.2019.119284

[14] Z. Huang, M. Fan, and H. Tian, "Rare earth elements of fly ash from Wyoming's Powder River Basin coal," *J. Rare Earths*, vol. 38, pp. 219–226, 2020.

[15] L. S. Morf, R. Gloor, O. Haag, M. Haupt, S. Skutan, F. D. Lorenzo, and D. Böni, "Corrigendum to "precious metals and rare earth elements in municipal solid waste – Sources and fate in a Swiss incineration plant"," *Waste Manage.*, vol. 33, 2013. https://doi.org/10.1016/j.wasman.2013.03.001

[16] J. Pan, B. V. Hassas, M. Rezaee, C. Zhou, and S. V. Pisupati, "Recovery of rare earth elements from coal fly ash through sequential chemical roasting, water leaching, and acid leaching processes," *J. Clean. Prod.*, vol. 284, no. 124725, 2020. https://doi.org/10.1016/j.jclepro.2020.124725

[17] R. S. Blissett, N. Smalley, and N. A. Rowson, "An investigation into six coal fly ashes from the united kingdom and poland to evaluate rare earth element content," *Fuel*, vol. 119, pp. 236–239, 2014. https://doi.org/10.1016/j.fuel.2013.11.053

[18] S. Dai, D. Ren, C.-L. Chou, R. B. Finkelman, V. V. Seredin, and Y. Zhou, "Geochemistry of trace elements in Chinese coals: A review of abundances, genetic types, impacts on human health, and industrial utilization," *Int. J. Coal Geol.*, vol. 94, pp. 3–21, 2012. https://doi.org/10.1016/j.coal.2011.02.003

[19] Z. Li, X. Li, L. Zhang, S. Li, J. Chen, X. Feng, D. Zhao, Q. Wang, Z. Gao, and B. Xiong, "Partitioning of rare earth elements and yttrium (REY) in five coal-fired power plants in Guizhou, Southwest China," *J. Rare Earths*, vol. 38, pp. 1257–1264, 2020. https://doi.org/10.1016/j.jre.2019.12.013

[20] P. Liu, R. Huang, and Y. Tang, "Comprehensive understandings of rare earth element (REE) speciation in coal fly ashes and implication for REE extractability," *Environ. Sci. Technol.*, vol. 53, pp. 5369–5377, 2019. https://doi.org/10.1021/acs.est.9b00005

[21] J. Pan, T. Nie, B. Vaziri Hassas, M. Rezaee, Z. Wen, and C. Zhou, "Recovery of rare earth elements from coal fly ash by integrated physical separation and acid leaching," *Chemosphere*, vol. 248, p. 126112, 2020. https://doi.org/10.1016/j.chemosphere.2020.126112

[22] R. K. Taggart, J. C. Hower, and H. Hsu-Kim, "Effects of roasting additives and leaching parameters on the extraction of rare earth elements from coal fly ash," *Int. J. Coal Geol.*, vol. 196, pp. 106–114, 2018. https://doi.org/10.1016/j.coal.2018.06.021

[23] Z. Wang, S. Dai, J. Zou, D. French, and I. T. Graham, "Rare earth elements and yttrium in coal ash from the Luzhou power plant in Sichuan, Southwest China: Concentration, characterization and optimized extraction," *Int. J. Coal Geol.*, vol. 203, pp. 1–14, 2019. https://doi.org/10.1016/j.coal.2019.01.001

[24] Z. Huang, M. Fan, and H. Tiand, "Coal and coal byproducts: A large and developable unconventional resource for critical materials – Rare earth elements," *J. Rare Earths*, vol. 36, pp. 337–338, 2018. https://doi.org/10.1016/j.jre.2018.01.002

[25] R. K. Taggart, J. C. Hower, G. S. Dwyer, and H. Hsu-Kim, "Trends in the rare earth element content of U.S.-based coal combustion fly ashes," *Environ. Sci. Technol.*, vol. 50, pp. 5919–5926, 2016. https://doi.org/10.1021/acs.est.6b00085

[26] P. Stabile, M. Bello, M. Petrelli, E. Paris, and M. R. Carroll, "Vitrification treatment of municipal solid waste bottom ash," *Waste Manag.*, vol. 95, pp. 250–258, 2019. https://doi.org/10.1016/j.wasman.2019.06.021

[27] L. Zhao, F. S. Zhang, and J. Zhang, "Chemical properties of rare earth elements in typical medical waste incinerator ashes in China," *J. Hazard. Mater.*, vol. 158, pp. 465–470, 2008. https://doi.org/10.1016/j.jhazmat.2008.01.091

[28] V. Funari, S. N. Bokhari, L. Vigliotti, T. Meisel, and R. Braga, "The rare earth elements in municipal solid waste incinerators ash and promising tools for their prospecting," *J. Hazard. Mater.*, vol. 301, pp. 471–479, 2016. https://doi.org/10.1016/j.jhazmat.2015.09.015

[29] Y. S. Shim, S. W. Rhee, and W. K. Lee, "Comparison of leaching characteristics of heavy metals from bottom and fly ashes in Korea and Japan," *Waste Manag.*, vol. 25, pp. 473–480, 2005. https://doi.org/10.1016/j.wasman.2005.03.002

[30] S. Mondal, A. Ghar, A. K. Satpati, P. Sinharoy, D. K. Singh, J. N. Sharma, T. Sreenivas, and V. Kain, "Recovery of rare earth elements from coal fly ash using TEHDGA impregnated resin," *Hydromet.*, vol. 185, pp. 93–101, 2019. https://doi.org/10.1016/j.hydromet.2019.02.005

[31] S. E. Perämäki, A. J. Tiihonen, and A. O. Väisänen, "Occurrence and recovery potential of rare earth elements in Finnish peat and biomass combustion fly ash," *J. Geochem. Explor.*, vol. 201, pp. 71–78, 2019. https://doi.org/10.1016/j.gexplo.2019.03.002

[32] J. Hower, J. Groppo, K. Henke, M. Hood, C. Eble, R. Honaker, W. Zhang, and D. Qian, "Notes on the potential for the concentration of rare earth elements and Yttrium in coal combustion fly ash," *Miner.*, vol. 5, pp. 356–366, 2015. https://doi.org/10.3390/min5020356

[33] S. K. Pandey and T. Bhattacharya, "Mobility, ecological risk and change in surface morphology during sequential chemical extraction of heavy metals in fly ash: A case study," *Environ. Technol. Inno.*, vol. 13, pp. 373–382, 2019. https://doi.org/10.1016/j.eti.2016.10.004

[34] X. Wan, W. Wang, T. Ye, Y. Guo, and X. Gao, "A study on the chemical and mineralogical characterization of MSWI fly ash using a sequential extraction procedure," *J. Hazard Mater.*, vol. 134, pp. 197–201, 2006. https://doi.org/10.1016/j.jhazmat.2005.10.048

[35] F. Zhu, Y. Xiong, Y. Wang, X. Wei, X. Zhu, and F. Yan, "Heavy metal behavior in 'Washing-Calcination-Changing with Bottom Ash' system for recycling of four types of fly ashes," *Waste Manag.*, vol. 75, pp. 215–225, 2018. https://doi.org/10.1016/j.wasman.2018.01.032

[36] B. Zawisza, K. Pytlakowska, B. Feist, M. Polowniak, A. Kita, and R. Sitko, "Determination of rare earth elements by spectroscopic techniques: A review," *J. Anal. Atom. Spectrom.*, vol. 26, no. 12, pp. 2373–2390, 2011. https://doi.org/10.1039/c1ja10140d

[37] Y. Zhang, Z. Jiang, M. He, and B. Hu, "Determination of trace rare earth elements in coal fly ash and atmospheric particulates by electrothermal vaporization inductively coupled plasma mass spectrometry with slurry sampling," *Environ. Pollut.*, vol. 148, pp. 459–467, 2007. https://doi.org/10.1016/j.envpol.2006.12.004

[38] R. Lin, B. Howard, E. Roth, T. Bank, E. Granite, and Y. Soong, "Enrichment of rare earth elements from coal and coal by-products by physical separations," *Fuel*, vol. 200, pp. 506–520, 2017. https://doi.org/10.1016/j.fuel.2017.03.096

[39] Z. Ma, X. Shan, and F. Cheng, "Distribution characteristics of valuable elements, Al, Li, and Ga, and rare earth elements in feed coal, fly ash, and bottom ash from a 300 mw circulating fluidized bed boiler," *ACS Omega*, vol. 4, pp. 6854–6863, 2019. https://doi.org/10.1021/acsomega.9b00280